J Mater Sci (2011) 46:38–46
DOI 10.1007/s10853-010-4793-9

INTERFACE SCIENCE

The effect of heat treatment temperature on the interfacial shear strength of C/C composites

Soydan Ozcan · Jale Tezcan · Bijay Gurung · Peter Filip

Received: 29 April 2010 / Accepted: 24 July 2010 / Published online: 10 August 2010

Abstract This paper investigates the effect of heat treatment temperature on the interfacial shear strength (IFSS) of carbon/carbon composites reinforced with polyacrylonitrile-based fibers. A series of single fiber push-out tests were performed on specimens heat treated at 1800, 2100, and 2400 °C, using a nanoindenter with a flat ended conical tip. The microstructure was characterized using polarized light and transmission electron microscopy and the debonded fiber/matrix interface was examined using scanning electron microscopy. Wavelet analysis of the load–displacement data was used as an additional tool to investigate the initiation and progression of debonding. Compared to 1800 °C, heat treatment at 2400 °C was associated with a decrease in IFSS, from 12 to 7 MPa. Transmission electron microscopy study showed that the microstructure of the fiber/matrix interphase remained amorphous even with heat treatment at 2400 °C. The decrease in the IFSS can be partly attributed to the reorganization of the graphene sheets in the matrix in the vicinity of fiber/matrix interphase. The thermal expansion mismatch between fiber and pyrocarbon matrix is another possible reason for the observed decrease in the IFSS.

S. Ozcan · B. Gurung · P. Filip
Mechanical Engineering and Energy Processes, Southern Illinois University, Carbondale, IL, USA

J. Tezcan
Civil and Environmental Engineering, Southern Illinois University, Carbondale, IL, USA

S. Ozcan · B. Gurung · P. Filip
Center for Advanced Friction Studies, Southern Illinois University, Carbondale, IL, USA

Present Address:
S. Ozcan (✉)
Materials Science and Technology Division, Oak Ridge National Laboratory, Oak Ridge, TN 37830, USA
e-mail: ozcans@ornl.gov

Introduction

Carbon fiber reinforced carbon matrix (C/C) composites offer significant advantages in high temperature braking and aerospace applications due to the superior mechanical and thermal properties at very high temperatures [1–5]. Hardly any material can match C/C composites when high specific strength, toughness, low thermal expansion, low density, and the ability to retain these properties at high temperatures are considered. Mechanical properties of C/C composites are greatly affected by the properties of fiber/matrix interface [6–13] in addition to the intrinsic properties of the fiber and the matrix [14–17]. A weak fiber/matrix interface is associated with high fracture toughness but lower strength and proportionality limit [18]. This behavior stems from the fact that the fiber/matrix interface provides an effective mechanism for hindering crack propagation, thereby limiting the damage to the reinforcing fiber. Therefore, interfacial shear strength (IFSS) constitutes an important factor in optimizing the C/C composites for specific uses.

Several test techniques, including micro-droplet fiber pullout, single fiber fragmentation, and single fiber push-out indentation, are available for the measurement of IFSS [19–23]. To date, extensive theoretical and experimental studies have been dedicated to the investigation of fiber/matrix interface. However, many of these studies were on polymer and ceramic matrix composites [24–28], only a few of them addressed the IFSS of C/C composites [29, 30].

Interfacial shear strength (IFSS) of C/C composites is determined in part by the processing conditions. High temperature treatment (HTT), generally being a part of the processing, can have a profound influence on the interface properties [31]. However, the mechanisms by which heat treatment influences the IFSS are not currently well-understood. At first look, one might expect a positive correlation between the two, mainly because of stress-induced graphitization [32], which induces a weak chemical bonding, in addition to the mechanical one, at high temperatures.

Several recent studies tried to establish a link between HTT and IFSS, but the findings have been largely inconclusive. Some earlier efforts focused on the pitch-fiber-reinforced composites. One such study reported an inverse relationship between the graphitization temperature and the IFSS, which was considered abnormal [33]. Results from another investigation based on pull-out tests were equally peculiar: The samples heat treated at 2000 °C had higher IFSS than the ones treated at 1200 and 2600 °C [34]. However, the researchers of this study caution that the reported IFSS represents only a small fraction of the tests, for which fiber pull-out was confirmed. Most tests with samples treated at higher temperatures resulted in fiber break or exfoliation, rather than fiber pull-out. More recently, bundle push-out tests on specimens heat treated at a wide range of temperatures showed a consistent decrease in IFSS with HTT [35]. This decrease was partly attributed to the extension of interfacial debonding, as confirmed by the scanning electron microscopy (SEM) images of the cross sections, due to the development of graphitization in the matrix [36].

Experimental results on composites reinforced with polyacrylonitrile (PAN)-based fibers have also been reported. In one study, the IFSS was maximum for the heat treatment temperature of 2100 °C, whereas it was lower for 1800 and 2400 °C [17]. This observation led to the idea of an optimal temperature, for which the fiber–matrix bonding is the strongest. In a more recent investigation, a 100% increase in the IFSS was measured with an increase of heat treatment temperature from 1800 to 2000 °C [37]. However, the IFSS for higher temperatures was not reported.

In spite of the studies reported to date, the causal relationship between HTT and IFSS in C/C composites has yet to be fully elucidated. Because of the large variation in the material composition, as well as the differences in specimen preparation and testing procedures, it is difficult to derive definitive conclusions from the studies conducted so far. Until there is consensus on proper testing procedures, supporting the test results with additional imaging and analytical techniques will be helpful.

In this paper, we investigate the effect of HTT on IFSS of C/C composites. A series of single fiber push-out tests were performed on specimens from a PAN fiber reinforced carbon matrix composite. The microstructure was characterized using imaging and the debonded fiber/matrix interface was examined using SEM. Wavelet analysis of the load–displacement data was used as an additional tool to investigate the initiation and progression of debonding.

Experimental procedures

The C/C composite used in this study was kindly provided by Honeywell Aircraft Landing System™ (ALS). The preform materials used to prepare the C/C composite are composed of needle-punched, non-woven mats of randomly oriented, pre-oxidized PAN-based fibers. The thickness of each mat is approximately 1 mm. In the finished product, about 10% of the fibers are oriented perpendicular to the plane of the mats. The preforms were heat stabilized, and then densified using chemical vapor infiltration (CVI) technique by Honeywell ALS. The composite samples were received in the form of disks with 600 mm diameter and 25 mm thickness. The density measured by helium pycnometry was 1.81 g/cm^3. Specimens with a rectangular cross section (70 mm × 35 mm) were cut from the disks, and heat treated in a graphitization furnace (Model: TP-4X10-G-G-D64A-A-27, Centorr Associates Inc). The heat treatment was performed in an argon protective atmosphere (∼0.5 bar) for 1 h at three different temperatures (1800, 2100, and 2400 °C). The corresponding sample notifications are given in Table 1. After the heat treatment at 1800, 2100, and 2400 °C, the density increased from 1.81 g/cm^3 to 1.97, 2.06, and 2.11 g/cm^3, respectively.

After the heat treatment, cubic specimens (15 × 15 × 15 mm^3) were cut from the rectangular samples, mounted into an epoxy resin, and polished using diamond slurries with a grain size ranging from 6 μm down to 0.25 μm. The polishing was completed using a 0.05 μm grain size alumina suspension. The microstructure of the polished samples was examined by polarized light microscopy (Nikon Eclipse LV 150), and the extinction angles of the different textures of pyrocarbons were measured. The activity of the optical regions is correlated with the orientation of the graphite lamellae. Based on the classification used in the

Table 1 Sample notifications and corresponding final heat treatment temperatures

Heat treatment temperature	Sample notification
1800 °C	CC-D18
2100 °C	CC-D21
2400 °C	CC-D24

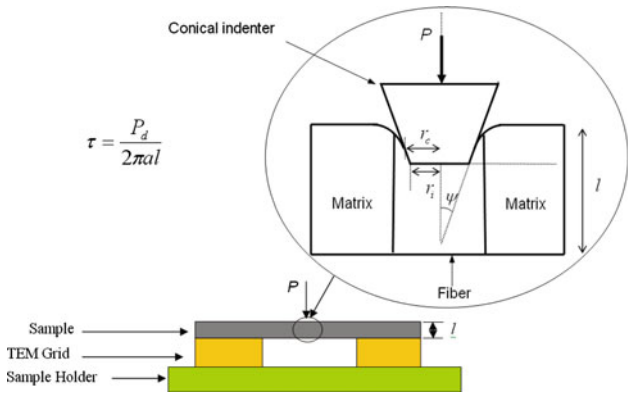

Fig. 1 Schematic of sample set-up and deformation during the push-out test in the nanoindenter

literature [38–43], the optical textures of pyrocarbons were described as: isotropic (A_e <4°), dark laminar (4° ≤ A_e < 12°), smooth laminar (12° ≤ A_e < 18°), and rough laminar (A_e ≥ 18°), where A_e is the extinction angle.

For the transmission electron microscopy (TEM) imaging, 300 μm thick foils were cut by linear precision diamond saw (Buehler, Isomet 4000). From these foils, 3 mm diameter disks were core-drilled (Core Drill, VCR Group, Model V 7110) and dimpled down to a thickness of about 5 μm (Dimpler, D 500i, VCR Group). The final thinning and polishing of the samples were done using the ion mill (Gatan, 691 Precision Ion Polishing System) with a beam at 4° angle at 3 keV. The TEM studies were carried out using a 200 kV transmission electron microscope (JEOL 2010 EF).

For push-out tests, three thin samples (~500 μm thick) were cut using diamond saw and polished down to the thickness of approximately 200 μm by using a polishing equipment (Buehler Minimet 1000, Model No: 69-1100). These samples were mounted on TEM copper grids using a crystal bond wax to form a beam and placed on the nanoindenter sample holder. Schematic of push-out testing set-up and deformation mechanism is given in Fig. 1.

The push-out tests were conducted at room temperature using a Nano Indenter® (XP system, MTS Nanoinstruments, Knoxville, TN), using a sixty degree cone indenter with a 5 μm diameter flat-end tip (Fig. 1). Twenty carbon fibers oriented perpendicular to the sample surface were randomly chosen from each sample. The surface of each sample was inspected by the Hitachi S570 scanning electron microscope (SEM) before the tests to select the fibers with proper orientation. A constant load rate of 0.66 mN/s was applied until the preset maximum load of 108 mN was reached. After the test, SEM imaging was used to eliminate measurements exhibiting fracturing of fiber or matrix. If push-out was not observed, the test was deemed unsuccessful, and was repeated using another fiber.

Results and discussion

Microstructure

Characteristic light microscopy images of samples after the push-out tests are shown in Fig. 2. Figure 2a shows a low magnification image in white light, while Fig. 2b is a polarized light micrograph showing the cross sections of the carbon fiber and the CVI matrix. The matrix exhibited a 20° extinction angle (A_e) indicating highly anisotropic pyrocarbon, which is receptive to develop graphite-like microstructure during HTT. As expected, carbon fibers did not exhibit any visible response to polarizer activity, indicating their turbostratic microstructure. The light microscopy images shown in Fig. 2 indicate good interfacial contact

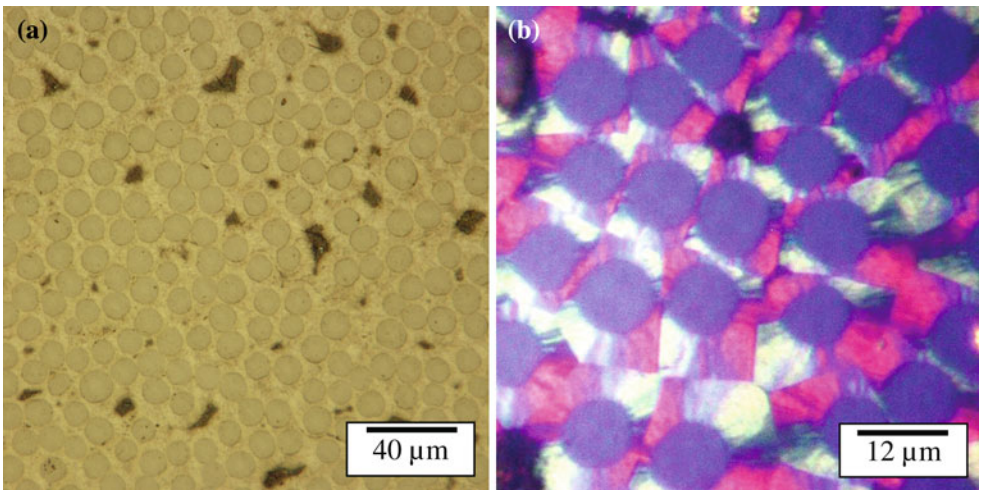

Fig. 2 Light microscopy image of polished surface showing carbon fiber cross sections at different magnifications. **a** CC-D18 and **b** CC-D24

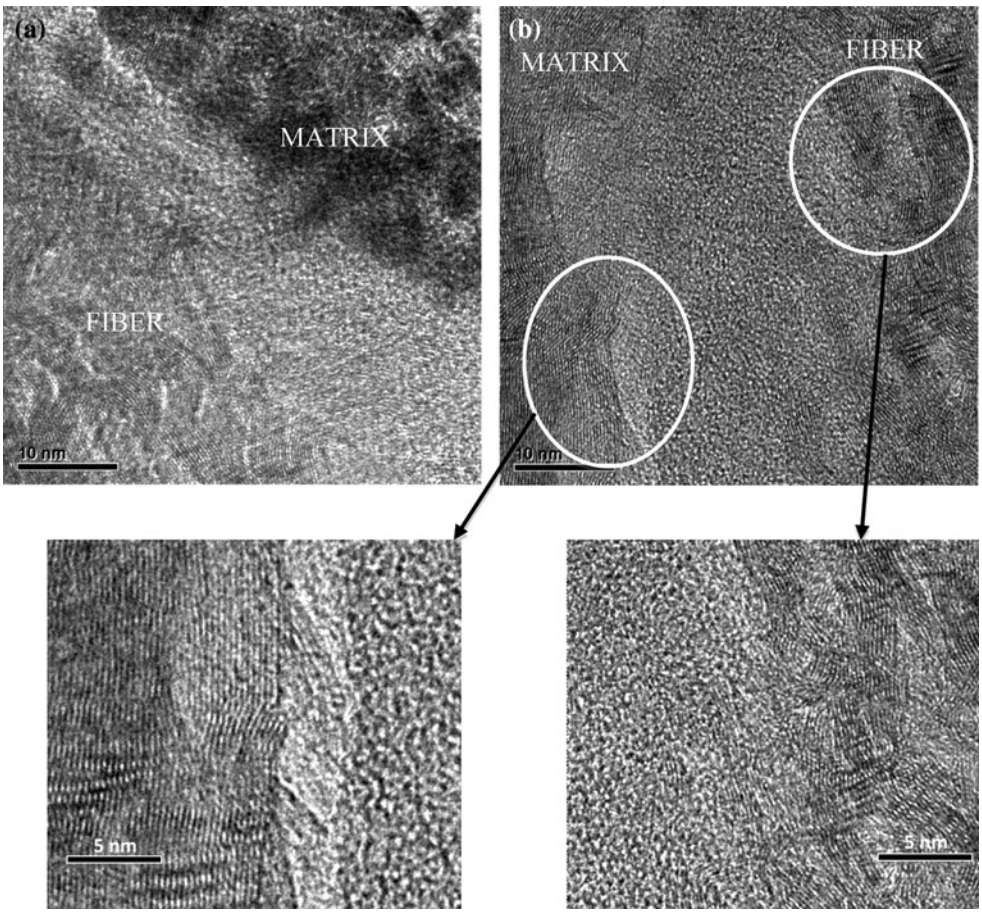

Fig. 3 TEM images of the fiber, matrix, and interphase of CC-D18 (**a**), CC-D21 with and high magnification 002 lattice fringe images (**b**)

between the fibers and the matrix. Pores (dark areas) are also visible on polished surface.

Characteristic TEM images of samples subjected to different heat treatment temperatures are given in Figs. 3 and 4. As the figures show, the fiber/matrix interphase consists of non-graphitizable isotropic carbon and this microstructure remains amorphous even after heat treatment at 2400 °C. Most of the graphene layers in the CVI matrix are oriented parallel to the fiber/matrix interphase, but the ones in the PAN fiber are randomly oriented. The graphene layers in the CVI are considerably longer than the ones in the PAN fibers.

After the push-out tests, SEM images of the specimens were taken to check for any visible damages to the fiber or the matrix, and to confirm that the debonding is complete and the fiber has been pushed out of the matrix. Typical SEM images are shown in Fig. 5. As the figure shows, the fiber has debonded from the matrix, and there is no evidence of cracking or damage to the fiber or the matrix.

Analysis of experimental data

In a typical push-out test, initiation of debonding is associated with a slope decrease in the load–displacement curve. However, identification of debonding from the load–displacement data is not always a straightforward task as the slope change at debonding initiation may be too subtle [26]. Moreover, even when the debonding load can be accurately detected, the determination of the IFSS is still challenging since the shear stress distribution over the interface may not be uniform.

In this study, the test results were classified according to the observed debonding behavior. Three debonding types were identified: (a) sudden and complete; (b) partial; and (c) progressive. The classification of debonding type was based on combined information from the load/displacement curve, SEM images, and wavelet transform of the push-out data.

Wavelet transform [44] is an analytical tool that decomposes a function into its multiscale components using basis functions which are scaled and shifted versions of a wavelet. Wavelet transform allows detection of critical points that are hidden in the signal itself, but apparent in the higher derivatives. With a properly selected wavelet, the coefficients corresponding to the smooth parts of the function will vanish and the discontinuities in the function will be localized by the remaining coefficients for all scales

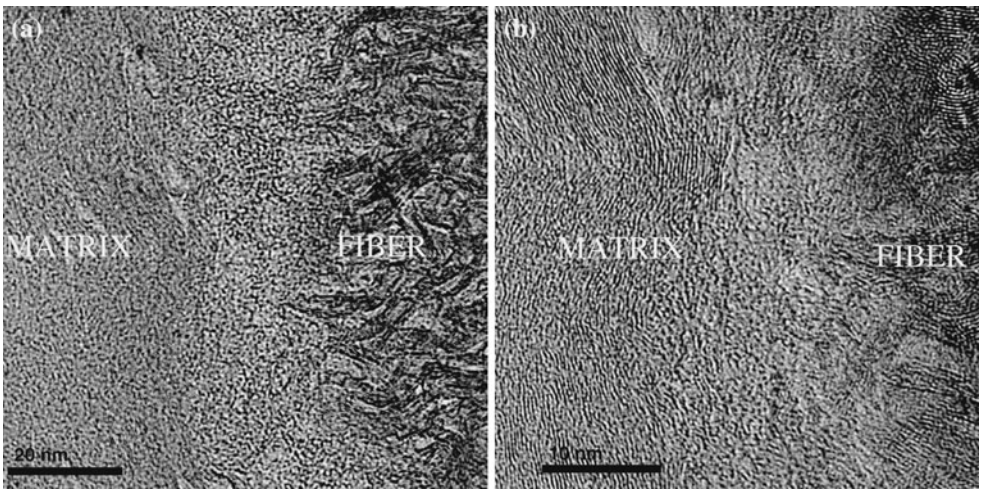

Fig. 4 TEM images of the fiber, matrix and interphase of CCD-24 (**a**, **b**). Amorphous interphases are visible between marked fibers and matrices in each image

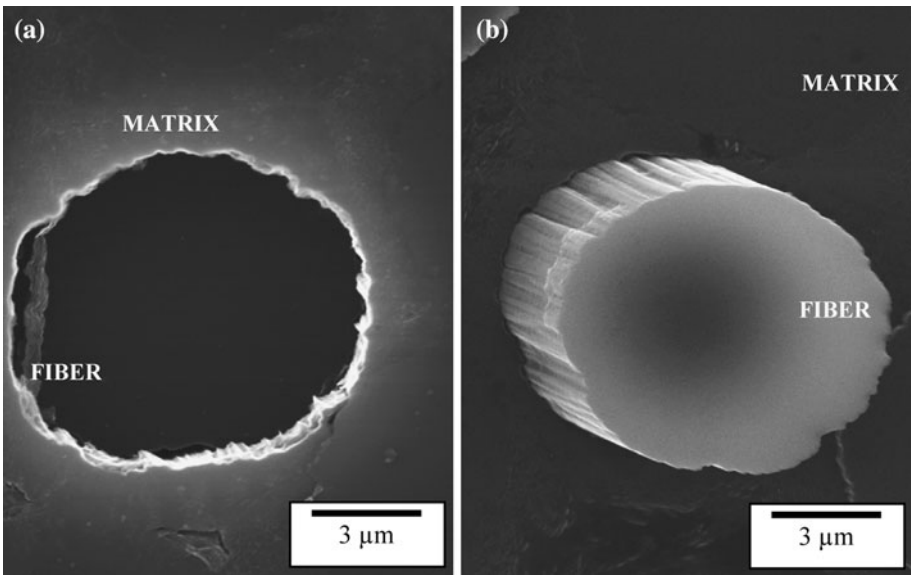

Fig. 5 SEM images taken after single fiber push-out tests. View from top (location of applied force) (**a**) and bottom (pushed out fiber from the matrix) (**b**)

[44]. In spite of being a relatively new tool, wavelet analysis has already been used in the evaluation of interfacial properties of composites [45]. In this study, Daubechies wavelets with four vanishing moments [46] were used in the analysis of the push-out data. The wavelet coefficients corresponding to the three levels (D1, D2, and D3) were used in locating the debonding load, and characterizing the debonding behavior.

Sudden and complete debonding of the fiber/matrix interface is likely for short fibers, when the samples are thin enough to allow propagation of interfacial cracks over the entire interface. In the load/displacement curve, a sudden increase in displacement at constant load indicates sudden debonding. In the plot of wavelet analysis, the coefficients attain their highest values around the debonding load and are negligibly small elsewhere. The completeness of debonding is confirmed when the residual displacement of the indenter tip matches the push-out distance observed in the SEM images.

Partial debonding occurs when the energy required to initiate debonding is smaller than the energy required for complete debonding, causing both bonded and debonded regions to be present at the fiber/matrix interface [47]. In the load/displacement curve, there may not be a significant deviation from the initial slope. Wavelet coefficients do not attain significant values around a single load value or a load range. SEM images do not show any evidence of fiber sliding or push-out.

Progressive debonding is associated with a significant deviation from the initial slope, although the point where the slope occurs may not be obvious. Progressive debonding is confirmed when wavelet coefficients attain large

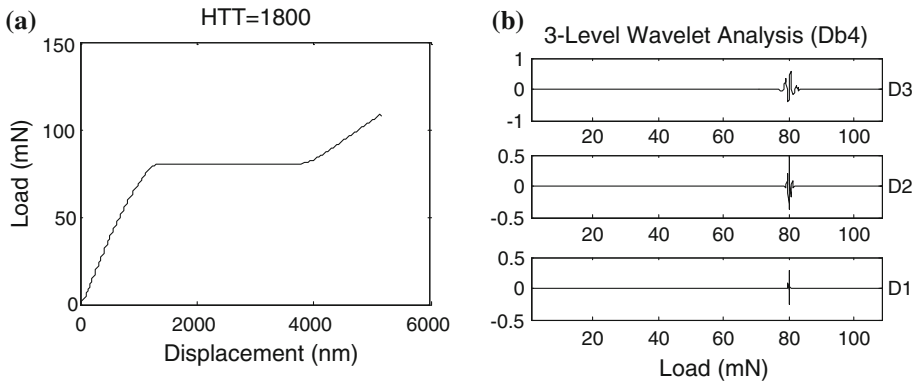

Fig. 6 Example of sudden and complete debonding for CC-D18 as measured by nanoindentation (**a**) and wavelet analysis (**b**)

values over a load range and the SEM images show that the fiber was pushed out.

Figure 6 demonstrates the applied load versus indentation displacement and its 3-level wavelet analysis for a sample treated at 1800 °C which exhibits sudden and complete debonding. The fiber slides under constant load (80 mN) until the indenter touches the matrix at around 3900 nm. The wavelet coefficients shown on the right hand side of the figure are concentrated around the load (∼80 mN) where the stiffness discontinuity occurs.

The advantage of wavelet transform becomes more obvious for cases where the fiber does not completely debond at a constant load. Figure 7 shows a case of partial debonding. The load–displacement plot shows a slope decrease between ∼50 and 100 mN, but does not indicate when debonding starts. On the other hand, the wavelet analysis shows that the debonding starts at approximately 90 mN, as evidenced by the attainment of the highest values of the wavelet coefficients at all levels. The slight slope increase at about 100 mN is visible in D1 level only, indicating a possible arrest of crack tip.

Figure 8 shows a case of progressive debonding; where the debonding is completed over the load range 70–85 mN. The increase in slope at around 95 mN coincides with the displacement when the conical indenter comes into contact with the matrix.

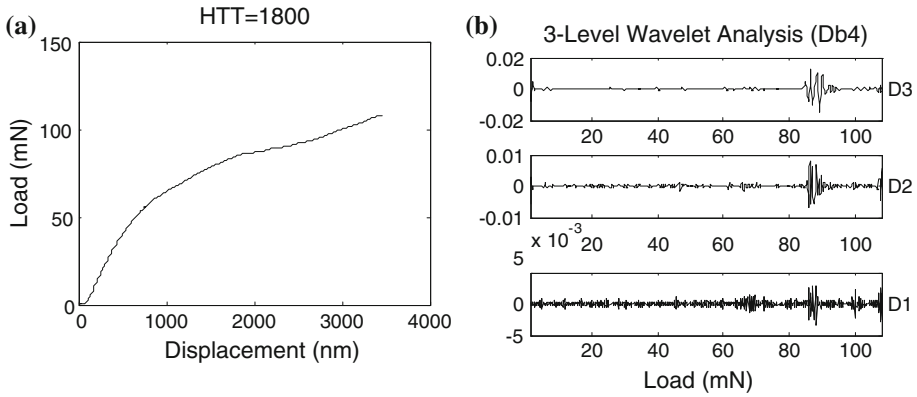

Fig. 7 Example of partial debonding for CC-D18 as measured by nanoindentation (**a**) and wavelet analysis (**b**)

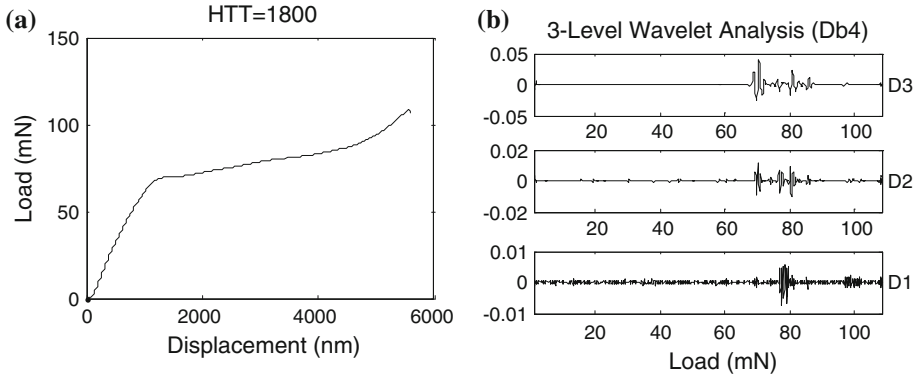

Fig. 8 Example of progressive debonding for CC-D18 as measured by nanoindentation (**a**) and wavelet analysis (**b**)

Similar plots corresponding to heat treatment temperatures of 2100 °C and 2400 °C are presented in Figs. 9, 10, 11 and 12, 13, 14, respectively.

The IFSS can be approximated as the average shear strength of the entire interface [22]

$$\tau = \frac{P_d}{2\pi a l} \quad (1)$$

where P_d, a, and l are the debonding load, radius of the fiber and the thickness of the specimen, respectively. Figure 15 shows the average IFSS with standard error bars for the samples subjected to HTT at 1800, 2100, and 2400 °C. The tests showing partial debonding were excluded from the IFSS calculations, since a debonding load cannot be identified in these tests.

While the average IFSS of CC-D21 and CC-D24 samples are about the same, there is a remarkable difference between the IFSS of CC-D18 and CC-D21 samples. The PAN fiber thermal shrinkage in both the axial and radial directions was reported at elevated temperatures [48]. As the CVI matrix expands at elevated temperatures it is expected that the thermal mismatch between the fiber and the matrix deteriorates the physical and/or chemical bonds at the fiber/matrix interphase. As seen in the TEM images

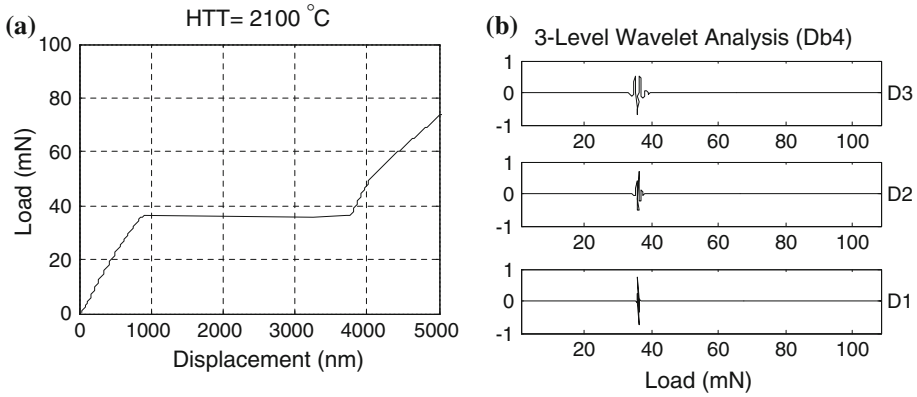

Fig. 9 Example of sudden and complete debonding for CC-D21 as measured by nanoindentation (**a**) and wavelet analysis (**b**)

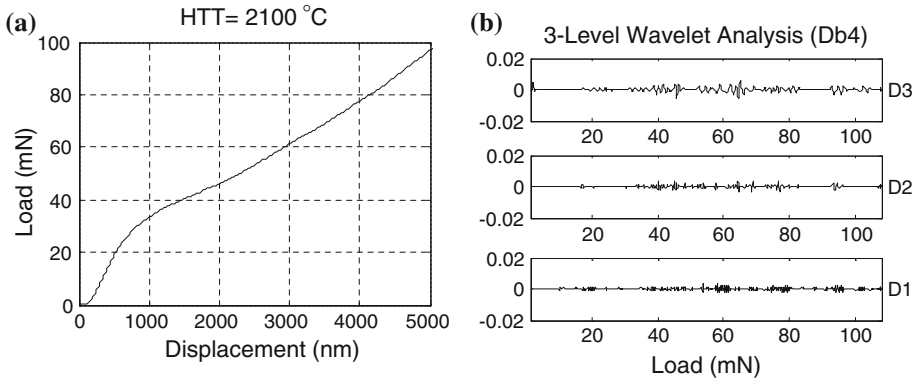

Fig. 10 Example of partial debonding for CC-D21 sample as measured by nanoindentation (**a**) and wavelet analysis (**b**)

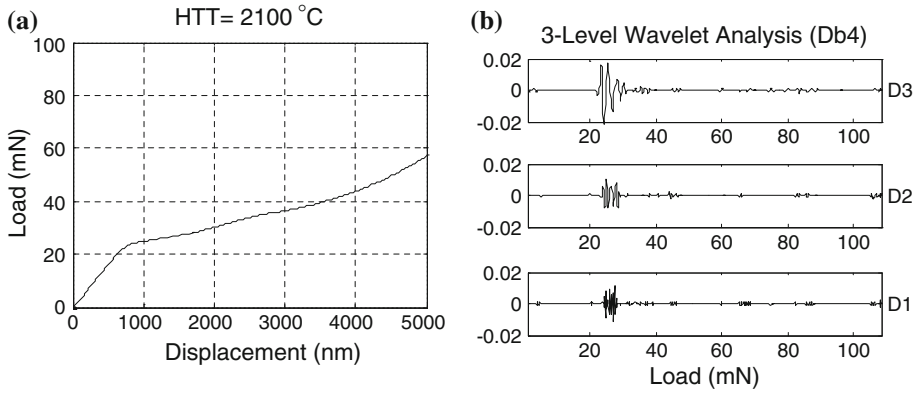

Fig. 11 Example of progressive debonding for CC-D21 sample as measured by nanoindentation (**a**) and wavelet analysis (**b**)

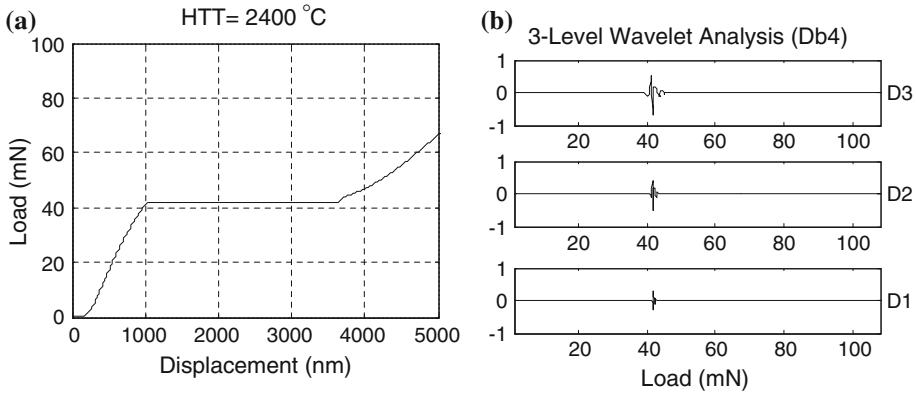

Fig. 12 Example of sudden and complete debonding for CC-D24 as measured by nanoindentation (**a**) and wavelet analysis (**b**)

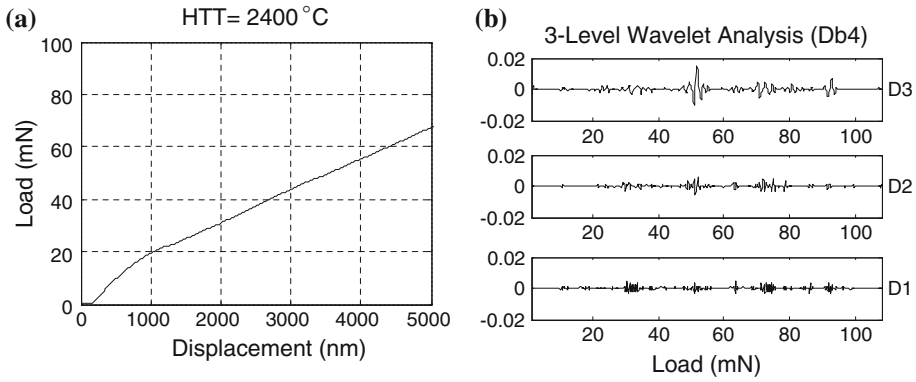

Fig. 13 Example of partial debonding for CC-D24 as measured by nanoindentation (**a**) and wavelet analysis (**b**)

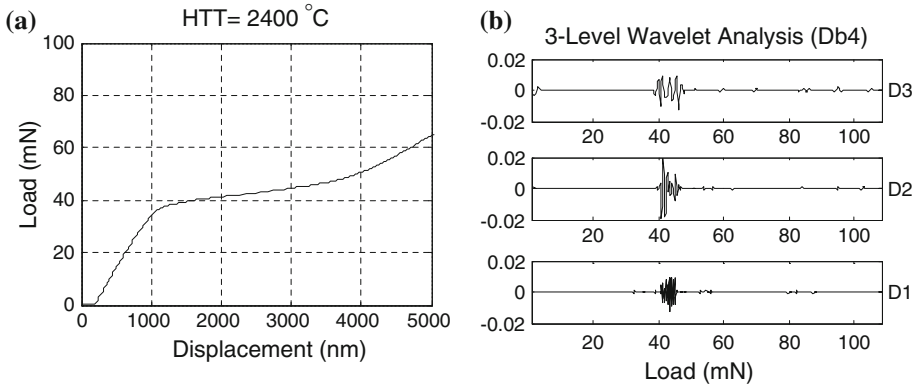

Fig. 14 Example of progressive debonding for CC-D24 as measured by nanoindentation (**a**) and wavelet analysis (**b**)

(Figs. 3, 4), only the microstructure of the highly anisotropic CVI matrix changes after the heat treatment at 2100 and 2400 °C. This formation of graphite-like carbon is due to the rearrangement of the carbon atoms and formation of well-organized crystallites. Extended flat aromatic layers of graphene sheets are arranged more or less parallel with respect to carbon fiber (Fig. 3b). These graphene sheets were arranged parallel to each other in columns, which in turn, were arranged parallel to the interphase (Fig. 4). This manner of arrangement has a major impact on IFSS. While the carbon atoms form very strong in-plane sp^2-bonds in the microstructure, they form weak out-of-plane π bonds. It is expected that in addition to the stresses due to the thermal mismatch, these microstructural changes in the CVI matrix will also reduce the IFSS. This is because of the low shear resistance between the CVI graphene sheets, adjacent to the fiber/matrix interphase.

PAN-based carbon fiber undergoes considerable dimensional changes (shrinking due to release of N and possibly H atoms trapped in the fiber) up to the temperature of 2000 °C [2, 49]. The volatilization is expected to be completed by 2100 °C. One possible reason for the slight increase in IFSS (Fig. 15) between 2100 and 2400 °C is the increase in the fiber/matrix contact area in CC-D24 caused by higher residual thermal stresses compared to CC-D21.

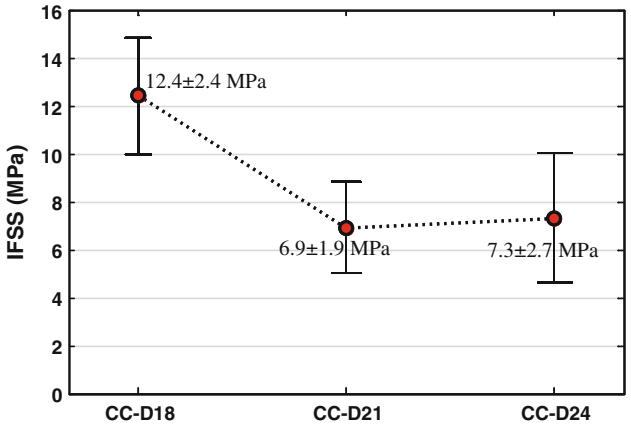

Fig. 15 Average IFSS with standard error bars of C/C composite samples heat treated at different temperatures

Conclusions

The C/C composites heat treated at 1800, 2100, and 2400 °C exhibited the presence of turbostratic PAN fiber and interphase with amorphous microstructure. The interphase microstructure remained unchanged after heat treatment. In contrast, the microstructure of the highly anisotropic CVI matrix changed significantly towards a better-ordered graphite-like carbon with increased treatment temperature. The fiber/matrix IFSS decreased after heat treatment at 2100 and 2400 °C compared to samples heat treated at 1800 °C. The decrease of IFSS was attributed to:

1. The thermal mismatch between the carbon fiber and the CVI matrix which deteriorates the interphase by introducing internal stresses and decreases the IFSS. This may also cause defects in the interphase.
2. Reorganization of carbon atoms in the CVI matrix and formation of extended graphene sheets with low shear resistance, arranged parallel to the fiber/matrix interphase.

Acknowledgement This research was sponsored by the National Science Foundation (Grant EEC 3369523372), State of Illinois and a consortium of 11 industrial partners of the Center for Advanced Friction Studies (http://frictioncenter.engr.siu.edu). The high-resolution TEM characterization was carried out at the Center for Microanalysis of Materials, University of Illinois, which is partially supported by the U.S. Department of Energy under grant DEFG02-91-ER45439.

References

1. Fitzer E, Manocha L (1998) Carbon reinforcements and carbon/carbon composites. Springer, New York
2. Savage G (1993) Carbon-carbon composites. Kluwer Academic Publishers, The Netherlands
3. Schmidt D, Davidson K, Theibert L (1999) SAMPE 35:47
4. Ozcan S, Filip P (2005) Wear 259:642
5. Chand S (2000) J Mater Sci 35:1303. doi:10.1023/A:1004780301489
6. Bradshaw W, Widoz A (1978) Ceram Bull 57:193
7. Cao H, Bischoff E, Sbaizero O et al (1990) J Am Ceram Soc 73:1691
8. Rice R, Spann J, Coblenz W (1984) Ceram Eng Sci Proc 5:614
9. Thouiess M, Sbaizero O, Sigl L, Evans A (1989) J Am Ceram Soc 72:525
10. Weihs T, Sbaizero O, Luh E, Nix W (1991) J Am Ceram Soc 74:535
11. Park S, Kim M (2000) J Mater Sci 35:1901. doi:10.1023/A:1004754100310
12. Ramirez F, Carlsson L, Acha B (2008) J Mater Sci 43:5230. doi:10.1007/s10853-008-2766-z
13. Zhang F, Wang R, He X, Wang C, Ren L (2009) J Mater Sci 44:3574. doi:10.1007/s10853-009-3484-x
14. Dillon F, Thomas K, Marsh H (1993) Carbon (New York, NY) 31:1337
15. Manocha L, Bahl O, Singh Y (1989) Carbon (New York, NY) 27:381
16. Ozcan S, Tezcan J, Filip P (2009) Carbon 47:3403
17. Domnanovich A, Peterlik H, Wanner A, Kromp K (1995) Compos Sci Technol 53:7
18. Grathwohl M (2001) Adv Eng Mater 3:371
19. Scheer R, Nairn J (1995) J Adhesion 53:45
20. Zhou X, Wagner H, Nutt S (2001) Composites A 32:1543
21. McDonough W, Antonucci J, He J et al (2002) Biomaterials 23:3603
22. Tezcan J, Ozcan S, Gurung B, Filip P (2008) J Mater Sci 43:1612. doi:10.1007/s10853-007-2333-z
23. Lee S, Nguyen T, Chin J, Chuang T (1998) J Mater Sci 33:5221. doi:10.1023/A:1004436021358
24. Faber K (1997) Annu Rev Mater Sci 27:499
25. Herrera-Franco P, Drzal L (1992) Composites 23:2
26. Kerans R, Parthasarathy T (1991) J Am Ceram Soc 74:1585
27. J Mandell, D Grande, T Tsaing, F McGarry (1986) ASTM International
28. Marshall D, Oliver W (1987) J Am Ceram Soc 70:542
29. Furukawa Y, Hatta H, Kogo Y (2003) Carbon 41:1819
30. Sakai M, Matsuyama R, Miyajima T (2000) Carbon 38:2123
31. Baudry P, Dourges M, Pailler R (2009) J Mater Sci 44:3643. doi:10.1007/s10853-009-3481-0
32. R Pleger, W Braue (1992) Advanced Aerospace Materials. Springer, Berlin, pp 203–218
33. Manocha L, Bahl O, Singh Y (1991) Carbon 29:351
34. Fujita K, Sakai H, Iwashita N, Sawada Y (1999) Composites A 30:497
35. Hatta H, Goto K, Ikegaki S, Kawahara I, Aly-Hassan M, Hamada H (2005) J Eur Ceram Soc 25:535
36. Hatta H, Goto K, Aoki T (2005) Compos Sci Technol 65:2550
37. Koyama M, Hatta H, Fukuda H (2005) Carbon 43:171
38. Diefendorf R, Tokarsky E. AF 33:615
39. Dupel P, Bourrat X, Pailler R (1995) Carbon 33:1193
40. Gray R (1966) J Nucl Mater 19:81
41. Pierson H, Lieberman M (1974) SLA-73-0925, Sandia Labs., Albuquerque, NM (USA); Sandia Labs., Livermore, CA (USA)
42. Bokros J, LaGrange L, Schoen F (1969) Chemistry and physics of carbon, vol 5. Dekker, New York, pp 1–118
43. Reznik B, Gerthsen D, Zhang W, Hüttinger K (2003) Carbon 41:376
44. Stark H (2005) Wavelets and signal processing: an application-based introduction. Springer, Berlin
45. Reed RP, Berg JC (2006) J Adhesion Sci Technol 20:1929
46. Daubechies I, Bates B (1993) J Acoust Soc Am 93:1671
47. Kim J, Mai Y (1998) Engineered interfaces in fiber reinforced composites. Elsevier Science, Oxford
48. Kulkarni R, Ochoa O (2006) J Compos Mater 40:733
49. Mittal J, Konno H, Inagaki M, Bahl O (1998) Carbon 36:1327